

Beam Loading in Magnicon Deflection Cavities

B. Hafizi and Steven H. Gold, *Fellow, IEEE*

Abstract—Analysis of the beam-deflection cavity interaction in a magnicon is presented and compared with experiment. For a driven cavity a dispersion relation is obtained wherein the interaction modifies the cold-cavity quality factor and the resonance frequency. In terms of a lumped-parameter equivalent circuit the interaction corresponds to a complex-valued beam admittance Y_b in parallel with the cavity admittance. The response of the gain cavities is modified by the same admittance. In a magnicon, Y_b is a sensitive function of the solenoidal focusing magnetic field B_0 , thus providing a convenient means of adjusting the cavity properties in experiments. When the relativistic gyrofrequency is twice the drive frequency, $\text{Im } Y_b = 0$ and the beam does not load the cavity. Analytical expressions of the variation of the detuning, instantaneous bandwidth (i.e., loaded quality factor) and gain with B_0 are derived. Simulation results are presented to verify the linear analysis with ideal beams and to illustrate the modifications due to finite beam emittance. Results of the magnicon experiment at the Naval Research Laboratory are examined in the light of the analysis.

Index Terms—Beam loading; electron beam defelection; emittance; energy spread; gain; magnicon; microwave tubes

I. INTRODUCTION

THE radio frequency (RF) source for the next linear collider (NLC) is required to generate a power of 1/2–1 GW per tube in a 200-ns pulse, or 100–200 J of energy in a pulse of up to a few μs in duration, at a frequency of 10–20 GHz [1]. It is generally believed that the efficiency of this RF source will have to be significantly better than that of the present generation of X-band klystrons. A variety of RF sources are under investigation at the present time aimed at fulfilling the needs of the NLC. These include the X-band klystron, gyroklystron, traveling-wave tube, harmonic converter, chopper-driven traveling-wave tube, and magnicon [2].

In scanning beam devices, such as the magnicon, phase synchronism between the transverse deflection of the beam and a rotating RF wave is created such that the interaction is invariant on the RF time-scale [3], [4]. This phase synchronism, which occurs without requiring beam bunching, makes possible very high efficiencies. In the magnicon circular scanning of a linear high-power pencil beam is effected by passing it through a series of cavities that are collectively referred to as the deflection system. The circularly scanned spiraling beam then enters an output cavity wherein RF power

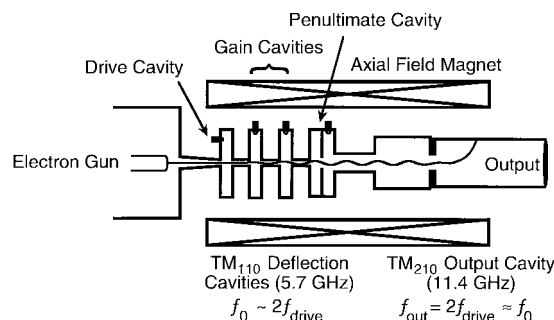


Fig. 1. Schematic of frequency-doubling magnicon amplifier operating at X-band (11.4 GHz); $f_0 \equiv |e|B_0/(2\pi\gamma mc)$ is the relativistic gyrofrequency in the axial magnetic field.

is generated by a gyroresonant mechanism. Achievement of high efficiency by means of a scanning beam interaction places a tight constraint on the beam quality as measured by the initial emittance and energy spread. Moreover, the beam quality must be preserved as much as possible as the beam is spun up in the deflection system, in the presence of the RF and nonideal effects such as fringing fields and self fields.

The operating principles of the magnicon may be illustrated by reference to the conceptual diagram in Fig. 1. A magnetized pencil beam from an electron gun transits a drive cavity containing a TM_{11} mode generated by an external RF source. The rotating magnetic field of the TM_{11} mode converts a small fraction of the beam axial momentum into transverse momentum, in such a way that the gyro-orbit grazes the cavity axis. The beam then enters a sequence of gain (or passive, or deflection) cavities, where the transverse motion creates RF fields that further deflect the beam, producing a progressively higher fraction of transverse momentum. This proceeds until the electrons exiting the final deflection cavity (also known as the penultimate cavity) have an α that exceeds unity, where α refers to the ratio of the transverse to parallel momentum.

As a result of the phase synchronous transverse deflection of the beam as a whole, the electrons entering the output cavity execute gyromotion whose entry point and guiding center rotate in space about the cavity axis at the drive frequency. The beam transverse motion is used to drive a gyroresonant fast-wave interaction in the output cavity. This interaction can be highly efficient because the electrons arrive in the cavity coherently gyrophased, thus providing for optimum energy transfer to a mode of the output cavity that rotates synchronously with the deflection cavity mode. The phase synchronism in the output cavity can take place at either the fundamental or a harmonic of the drive frequency. The magnicon program at the Naval Research Laboratory (NRL), Washington, DC, employs a frequency-doubling configuration,

Manuscript received May 30, 1996; revised October 7, 1996. This work was supported in part by the Division of High Energy Physics, Office of Energy Research, U.S. Department of Energy under Interagency Agreement DE-AI02-94ER-40861 and in part by the U.S. Office of Naval Research.

B. Hafizi is with ICARUS Research, Inc., Bethesda, MD 20824-0780 USA. S. H. Gold is with the Beam Physics Branch, Plasma Physics Division, Naval Research Laboratory, Washington, DC 20375-5346 USA.

Publisher Item Identifier S 0093-3813(97)01697-4.

with the output cavity operating in the TM_{210} mode at the second harmonic of the drive frequency (i.e., $2 \times \omega$, where ω is the drive frequency), but in the first harmonic of the gyrofrequency, ω_c [defined following (2)]. The synchronism condition in the deflection system cavities is $\omega \approx \omega_c/2$, while in the output cavity it is $2\omega \approx \omega_c$. This variant of the magnicon has several advantages, including the near-uniformity of the axial magnetic field throughout the circuit.

The NRL experiment has employed a single-shot Marx generator to power a plasma-induced field emission diode. A two deflection cavity, low drive power experiment employing a 1/2 MV, 200 A, 5.5 mm-diameter electron beam was initially performed, verifying the predictions of theory [5]. Recent experiments have demonstrated megawatt-level output power in a complete, five cavity device [6].

Although the magnicon has the potential of high average power at high efficiency, the technology on which it is based is less developed than either the traveling-wave tube, the klystron or the gyroklystron. There is also much that needs to be learned from the theoretical standpoint in order to derive scaling relations and be able to design experiments with confidence.

The theoretical work at NRL has concentrated on understanding the physics issues involved in the magnicon amplifier [4], [7]–[11]. In an early study a detailed linear analysis of the deflection system was presented. In particular, a general expression for the gain and frequency shift was obtained. An interesting aspect of magnicon behavior is the variation of the gain and frequency shift with the strength of the axial magnetic field. This allows one to control the cavity quality factor Q in experiments. Here, we shall present a description of beam loading effects in the deflection system. Use is made of the dispersion relation derived in the prior work, based on the Vlasov–Maxwell system of equations. This first principles analysis is extremely powerful and allows the determination of the loaded Q , i.e., the instantaneous bandwidth, the frequency shift and the gain over a broad range of magnetic fields, including the synchronous value. The analysis is also used to identify the equivalent-circuit parameters. Simulation results are presented to illustrate the validity of the linear analysis and modifications due to finite beam emittance. Finally, results of the NRL gain experiment are compared with the theory. The role of beam loading in the magnicon was first pointed out in [3], although its variation as a function of the magnetic field was not discussed. The first detailed analysis of beam loading was presented in [13], making use of the induced-current method in conjunction with a lumped equivalent circuit. The frequency response of the amplitude and phase of a gain cavity was determined for several values of magnetic field. However, this involved an iterative process that was not always stable.

II. DISPERSION RELATION

The ideal TM_{110} rotating mode in a cylindrical cavity may be represented by the vector potential

$$A_z = \frac{E_0 c}{i\omega} J_1\left(\frac{p_{11} r}{a}\right) \exp(i\phi - i\omega t) + \text{c.c.} \quad (1)$$

where r , ϕ , and z denote the cylindrical coordinates, E_0 is a constant, c is the speed of light, ω is the angular frequency, J_1 is the ordinary Bessel function of the first kind of order one, p_{11} is the first zero of J_1 , a is the cavity radius, the cutoff wavenumber is defined by $k_c \equiv p_{11}/a = \omega/c$, and c.c. means complex conjugate. In this paper centimeter-gram-second (CGS) units are used unless stated otherwise.

To obtain the dispersion relation the paraxial limit is considered; i.e., it is assumed that $v_x/v_z, v_y/v_z \ll 1$, and $r/a \ll 1$, where $\mathbf{v} = (v_x, v_y, v_z)$ is the velocity. Then, in the presence of a uniform axial magnetic field B_0 , the equations of motion of an electron are given by

$$\frac{d}{dt} v_{\perp} = i\omega_c v_{\perp} - i\omega_e v_{z0} \exp(i\omega t) \quad (2)$$

where $v_{\perp} = v_x + iv_y$, $\omega_c = |e|B_0/\gamma_0 mc$ is the relativistic gyrofrequency, $\omega_e = |e|E_0/\gamma_0 mc$, and e is the charge on an electron. Equation (2) is valid provided the signal strength is sufficiently small that the relativistic mass factor γ_0 and the longitudinal velocity v_{z0} may be supposed to be constants. Defining $x_{\perp} = x + iy$, and denoting by t_0 the time at which the electron enters the cavity, the solution of (2) with the initial conditions $x_{\perp}(t = t_0) = x_{\perp 0}$ and $v_{\perp}(t = t_0) = v_{\perp 0}$ is

$$x_{\perp} = x_{\perp 0} + \frac{v_{\perp 0}}{i\omega_c} \left[\exp\left(\frac{i\pi\omega_c}{\omega}\right) - 1 \right] + \frac{\omega_e v_{z0}}{i(\omega - \omega_c)} \exp(i\omega t_0) \cdot \left[\frac{2}{\omega} + \frac{\exp\left(\frac{i\pi\omega_c}{\omega}\right) - 1}{\omega_c} \right] \quad (3)$$

$$v_{\perp} = v_{\perp 0} \exp\left(\frac{i\pi\omega_c}{\omega}\right) + \frac{\omega_e v_{z0}}{\omega - \omega_c} \left[\exp\left(\frac{i\pi\omega_c}{\omega}\right) + 1 \right] \exp(i\omega t_0). \quad (4)$$

These equations express the values at the cavity exit, which, in terms of the transit angle $\theta = \omega(t - t_0) \approx (\omega/v_{z0})z$ is identified by $\theta = \pi$. For this value of transit angle the transverse excursion is a maximum. Equations (3) and (4) define the initial conditions at the entrance to the following drift tube.

In the drift region the beam orbit grazes the z -axis at a transit angle $\theta_d = \pi/2$, and completes one gyrational motion at $\theta_d = \pi$. Here, $\theta_d = \omega(t - t_0 - \pi/\omega)$ is the transit angle measured in the drift region. The length of the drift region determines the initial conditions for the gain cavity. The appropriate choice is $\theta_d = \pi/2$ and the beam enters that cavity, on axis, at $t_1 = t_0 + \pi/\omega + \pi/\omega_c$.

In the gain cavity we define $\omega'_e = |e|E'_0 \exp(i\varphi^*)/\gamma_0 mc$, where $E'_0 \exp(-i\varphi)$ is the amplitude—replacing E_0 in (1)—and * indicates the c.c. The orbit in the gain cavity

is given by

$$\begin{aligned}
 x_{\perp} = & x_{\perp 0} - \frac{v_{\perp 0}}{i\omega_c} \left[\exp \left(\frac{i\pi\omega_c}{\omega} \right) + 1 \right] \\
 & - \frac{v_{\perp 0}}{i\omega_c} \{ \exp [i\omega_c(t - t_1)] - 1 \} \exp \left(\frac{i\pi\omega_c}{\omega} \right) \\
 & - \frac{v_{z0}\omega'_e}{i(\omega - \omega_c)} \exp(i\omega t) \\
 & \times \left\{ \frac{1}{\omega} - \left(\frac{1}{\omega} - \frac{1}{\omega_c} \right) \exp[-i\omega(t - t_1)] \right. \\
 & \left. - \frac{1}{\omega_c} \exp[i(\omega_c - \omega)(t - t_1)] \right\} \\
 & - \frac{v_{z0}\omega_e}{i(\omega - \omega_c)} \exp(i\omega t) \exp \left(\frac{-i\pi\omega}{\omega_c} \right) \\
 & \times \left\{ 2 \left(\frac{1}{\omega} - \frac{1}{\omega_c} \right) \exp[-i\omega(t - t_1)] \right. \\
 & \left. - \frac{1 + \exp \left(\frac{i\pi\omega_c}{\omega} \right)}{\omega_c} \exp[i(\omega_c - \omega)(t - t_1)] \right\}. \quad (5)
 \end{aligned}$$

To assess the effects of beam loading it is necessary to solve the wave equation with the source term evaluated with the aid of the orbit in (5). Following [7], the current density for a monoenergetic beam of electrons with energy γmc^2 may be written as

$$\begin{aligned}
 J_z = & -I \int d^2r_{\perp 0} d^3p_0 f(\mathbf{r}_{\perp 0}, \mathbf{p}_0) \delta(\gamma_0 - \gamma) \\
 & \cdot \delta\{\mathbf{r}_{\perp} - \tilde{\mathbf{r}}_{\perp}[t, t_1(\mathbf{r}_{\perp 0}, \mathbf{p}_0, t, z)]\}
 \end{aligned}$$

where I is the beam current, $\tilde{\mathbf{r}}_{\perp}$ is the orbit in the x - y plane, expressed as a function of the time t and the entry time t_1 into the cavity, and $f(\mathbf{r}_{\perp 0}, \mathbf{p}_0)$ is the electron distribution—which is a function of the initial coordinates \mathbf{r}_0 and momenta \mathbf{p}_0 —subject to the normalization condition $\int d^2r_{\perp 0} d^3p_0 f(\mathbf{r}_{\perp 0}, \mathbf{p}_0) \delta(\gamma_0 - \gamma) = 1$. It is thus necessary to solve the wave equation

$$\left(\nabla^2 - \frac{1}{c^2} \frac{\partial^2}{\partial t^2} \right) A_z = -\frac{4\pi}{c} J_z$$

with the orbit given by (5) inserted into the expression for the current density. The solution of the wave equation can be readily obtained by substituting a vector potential of the form given in (1) into the left-hand side. For the right-hand side use is made of the orbit in (5) to evaluate the current density J_z . Since this calculation is standard [4], [7], for brevity, we quote the result from [7]. For an azimuthally symmetric distribution function and in the paraxial approximation the ratio of the electric field in the gain cavity to that in the drive cavity is given by

$$\frac{E'_0}{E_0} = \frac{\epsilon P}{-\epsilon D_r + \frac{d\epsilon_r}{dt} - i \left(\frac{1}{2Q} + \epsilon D_i \right)} \quad (6)$$

where

$$\begin{aligned}
 P_r = & \frac{-1}{\frac{\omega_c}{\omega}} \left[\frac{1}{1 - \frac{\omega}{\omega_c}} - \frac{\sin \theta_L}{\theta_L} - \frac{\sin \left(\frac{\omega_c}{\omega} - 1 \right) \theta_L}{\left(\frac{\omega_c}{\omega} - 1 \right)^2 \theta_L} \right], \\
 P_i = & \frac{-1}{\frac{\omega_c}{\omega}} \left[\frac{\sin^2 \left(\frac{\theta_L}{2} \right)}{\frac{\theta_L}{2}} - \frac{\sin^2 \left(\frac{\omega_c}{\omega} - 1 \right) \frac{\theta_L}{2}}{\frac{\left(\frac{\omega_c}{\omega} - 1 \right)^2 \theta_L}{2}} \right], \\
 D_r = & \frac{-\exp \left(\frac{-i\pi\omega}{\omega_c} \right)}{\frac{\omega_c}{\omega}} \left[2 \frac{\sin \theta_L}{\theta_L} - \left[1 + \exp \left(\frac{i\pi\omega_c}{\omega} \right) \right] \right. \\
 & \left. \cdot \frac{\sin \left(\frac{\omega_c}{\omega} - 1 \right) \theta_L}{\left(\frac{\omega_c}{\omega} - 1 \right)^2 \theta_L} \right], \\
 D_i = & \frac{\exp \left(\frac{-i\pi\omega}{\omega_c} \right)}{\frac{\omega_c}{\omega}} \left[2 \frac{\sin^2 \left(\frac{\theta_L}{2} \right)}{\frac{\theta_L}{2}} + \left[1 + \exp \left(\frac{i\pi\omega_c}{\omega} \right) \right] \right. \\
 & \left. \cdot \frac{\sin^2 \left(\frac{\omega_c}{\omega} - 1 \right) \frac{\theta_L}{2}}{\frac{\left(\frac{\omega_c}{\omega} - 1 \right)^2 \theta_L}{2}} \right].
 \end{aligned}$$

Here, $\theta_L = \omega L/v_z$, L is the length of the cavity, $\epsilon = [\beta_z/p_{11} J_2(p_{11})]^2 I/I_A$, $I_A = 1.7 \times 10^4 \gamma \beta_z$ is the Alfvén current, $\beta_z = v_z/c$, and $v_z = \int d^3p_0 v_{z0} f(\mathbf{r}_{\perp 0}, \mathbf{p}_0)$ is the mean axial velocity. In writing (6) the imaginary part of the frequency, $d\varphi/dt \equiv d\varphi_r/dt + id\varphi_i/dt$, has been absorbed in the definition of the cold cavity quality factor Q . Additionally, it has been assumed that $f(\mathbf{r}_{\perp 0}, \mathbf{p}_0) = \delta(p_{z0} - p_z) \delta(\mathbf{p}_{\perp 0}) \delta(\gamma_0 - \gamma)$. The simulations to be presented later extend this simplified model by employing a beam with finite emittance.

The parameter ϵ is proportional to the beam current. Beam loading effects are manifested through the terms involving ϵ in (6). Setting the real and the imaginary parts of the denominator in (6) separately equal to zero allows us to identify the resonant frequency ω_{res} and the loaded Q , Q_L

$$\omega_{res} = ck_c(1 + \epsilon D_r) \quad (7)$$

$$\frac{1}{Q_L} = \frac{1}{Q} + 2\epsilon D_i \quad (8)$$

where ck_c is the cold cavity frequency.

III. EQUIVALENT CIRCUIT

This section presents a brief summary of the lumped-element equivalent circuit for the gain cavity of a magnicon operating in the TM₁₁₀ mode. In this section SI units are used exclusively. The circuit is shown in Fig. 2. For the TM₁₁₀

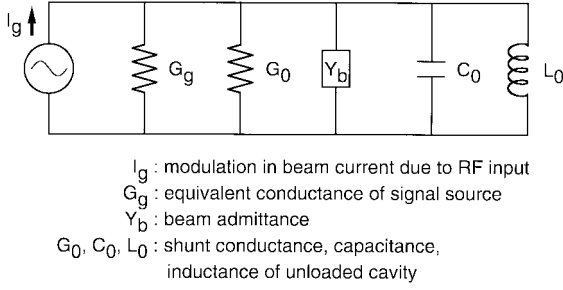


Fig. 2. Deflection cavity equivalent circuit. I_g : modulation in beam current due to RF input; G_g : equivalent conductance of signal source; G_0, C_0, L_0 : conductance, capacitance, and inductance of unloaded cavity; Y_b : beam admittance.

mode the Ohmic quality factor is given by

$$Q = \frac{\frac{p_{11}}{k_c \delta}}{1 + \frac{a}{L}} \quad (9)$$

where δ is the skin depth [14]. The shunt conductance G_0 is obtained by making use of $P_l = V^2 G_0 / 2$, where P_l is the power loss in the TM_{110} mode—which involves the Q —and V is the ac voltage. The latter is approximated by the product of the cavity length and the maximum of the axial electric field. Thus

$$G_0 \approx \frac{\pi Y_0}{Q k_c L} \left[\frac{p_{11} J_0(p_{11})}{J_1(p'_{11})} \right]^2 \approx \frac{1 + \frac{a}{L}}{\frac{65L}{\delta}}$$

where $Y_0 \approx (120\pi)^{-1} S$ is the admittance of free space and p'_{11} is the first zero of the derivative of J_1 . From the known values of Q and the conductance G_0 the capacitance and the inductance, C_0 and L_0 , respectively, are obtained from $\omega_{110} C_0 = Q G_0$ and $\omega_{110}^2 L_0 C_0 = 1$, where $\omega_{110} \equiv c k_c$.

The beam admittance is given by [3] $Y_b = 2\epsilon\omega_{110} C_0 (D_i + iD_r)$, which can be reexpressed as

$$Y_b = \frac{I}{V_0} \frac{\gamma_0 - 1}{\gamma_0} \frac{D_i + iD_r}{2\theta_L J_1^2(p'_{11})}$$

where $V_0 = (\gamma_0 - 1)mc^2/|e|$ is the dc beam voltage and θ_L is defined following (6).

The total admittance of the equivalent circuit is then given by $Y = G_0 - 2i\Delta\omega C_0 + Y_b$, where $\Delta\omega = \omega - \omega_{110}$ is the detuning from the cold cavity resonance frequency. From circuit theory it then follows that the frequency shift is given by

$$\Delta\omega = \frac{\text{Im } Y_b}{2C_0} = \epsilon\omega_{110} D_r$$

and the beam contribution to the quality factor is given by

$$\frac{1}{Q_b} = \frac{\text{Re } Y_b}{\omega_{110} C_0} = 2\epsilon D_i.$$

The latter two expressions are consistent with (7) and (8) given at the end of Section II.

In the magnicon $D_r < 0$ when the beam loading effect is capacitive and the frequency is down-shifted. Further, examination of the expression for D_i indicates that

$$\begin{aligned} Q_b &> 0, & \text{for } \omega_c < 2\omega \\ Q_b &= 0, & \text{for } \omega_c = 2\omega \\ Q_b &< 0, & \text{for } \omega_c > 2\omega. \end{aligned}$$

It is this particular characteristic of beam loading that is of interest since it allows one to control the effective cavity Q with relative ease in experiments. Note that the last of these conditions may lead to oscillation for sufficiently large beam loading. (See [14] for comparison with the equivalent circuit of a klystron.)

IV. SIMULATIONS AND COMPARISON WITH EXPERIMENT

The analysis in Section II may be employed to evaluate the beam-loading effect for realistic electron beams, i.e., with finite emittance. Choosing an appropriate form for the electron-distribution function at the entrance to the drive cavity, the relevant integrals may be performed to determine the gain. In practice the form of a realistic beam distribution is sufficiently complicated to require numerical evaluation of the integrals. The analysis was based on the assumption that the electron energy and axial velocity were relatively constant in the deflection cavities. This is a good assumption when the synchronism condition, $\omega_c = 2\omega$, is approximately valid, since there is little exchange of energy between the electrons and the RF. This will also emerge in the following discussion. However, away from synchronism and for large input drive, there may be significant transfer of energy and the linearized approach fails. It is therefore important to supplement the analysis with numerical solutions.

The steady-state code solves the equations of motion of a collection of electrons through given, ideal-cavity TM_{110} RF fields and the axial magnetic field using a fourth-order Runge-Kutta method. The RF field amplitude is made self-consistent by iteration, for given beam current and cavity losses. The code simulates a deflection system that consists of a drive and a gain cavity, interconnected by a drift tube.

In the ideal case the simulations employ a beam that is cold, with vanishing radius, at the entrance to the drive cavity. The parameters for the simulations are listed in Table I. Note that the Q value listed in Table I is much less than the purely ohmic Q predicted by (9). The listed Q includes the effects of RF coupling pickups [5]. The Q value employed in the simulations is rounded up to 1000, which is within the accuracy of measurements. Additionally it should be remarked that the experimentally-determined frequency of the actual cavity—including openings to beam tunnels and coupling pin holes—is about 5 MHz less than that listed in Table I. Finite-emittance simulations employ an initial distribution that represents the beam from a realistic diode using an electron optics code [15]. The beam is modeled as three concentric annuli, each with a given value of radius, beam α , and current, as listed in Table II.

Fig. 3 reproduces the measured gain data from [5] for a configuration of a drive cavity followed by a single gain cavity.

TABLE I
PARAMETERS FOR MAGNICON BEAM LOADING CALCULATION

Voltage	500 kV
Current I	172 A
Cavity Radius	3.2 cm
Cavity Length	2.26 cm
Quality Factor Q	1000
Drift Tube Length	1.13 cm
Input Power	10 kW
Cold Cavity Frequency $ck_c/2\pi$	5.712 GHz
Synchronous Magnetic Field B_0	8.074 kG

TABLE II
BEAM PARAMETERS FOR A MAGNICON DEFLECTION SYSTEM

Inner Shell	
Radius	0.8 mm
α	0.012
Current	26 A
Central Shell	
Radius	1.9 mm
α	0.0165
Current	52 A
Outer Shell	
Radius	2.75 mm
α	0.022
Current	94 A

TABLE III
LORENTZIAN FIT TO EXPERIMENTAL GAIN DATA

	Polarization 1	Polarization 2
Cold Cavity Quality Factor	970	950
Cold Cavity Frequency	5.680 GHz	5.6805 GHz
G_0	14.87 ± 1.06 dB	11.32 ± 0.86 dB
f_{L0}	5.6711 ± 0.0005 GHz	5.6701 ± 0.0003 GHz
Q	940 ± 168	1181 ± 159

The measurements of the *rotating* TM_{11} mode were carried out in the two separate *linear* polarizations, resulting in the data labeled Polarization 1 and Polarization 2. The statistical error bars from the original figure are duplicated, corresponding to the standard deviation of the mean of three to five shots for each frequency, except that minimum error bar size was set at ± 0.5 dB, so that the weighting of the points in the fits described below would not be unduly biased by the occurrence of a very small statistical spread at some frequencies. Each polarization was fit to a Lorentzian distribution, according to the formula

$$G(f) = G_0 + 10 \log \frac{f_{L0}^2}{f_{L0}^2 + 4Q^2(f - f_{L0})^2}$$

where G_0 is the gain in dB at the center frequency f_{L0} . A least squares fitting process, with the weighting of each point inversely proportional to the square of the size of the error bar, was employed to determine the three parameters G_0 , Q , and f_{L0} for each polarization. Table III lists the best-fit values for the parameters and the two curves in Fig. 3 show the Lorentzian fits.

Fig. 4 shows the power gain plotted as a function of the axial magnetic field. The solid curve is obtained from

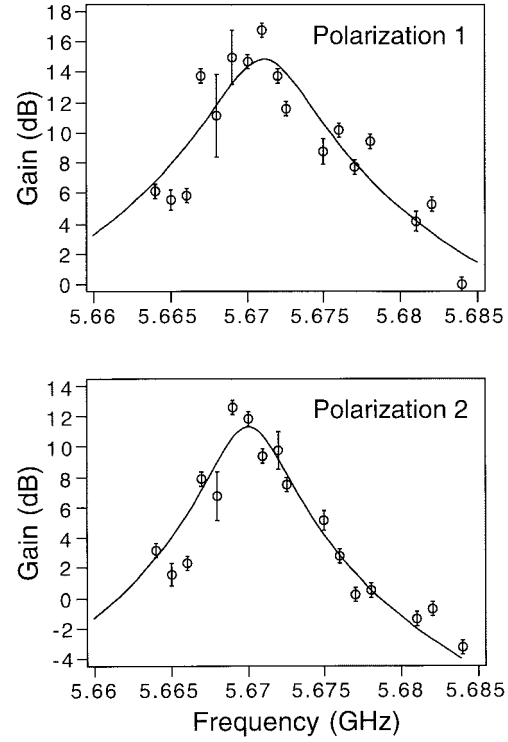


Fig. 3. Measured gain data for Polarization 1 and Polarization 2 that make up a rotating TM_{11} mode. The curves are least squares Lorentzian fits to the data points.

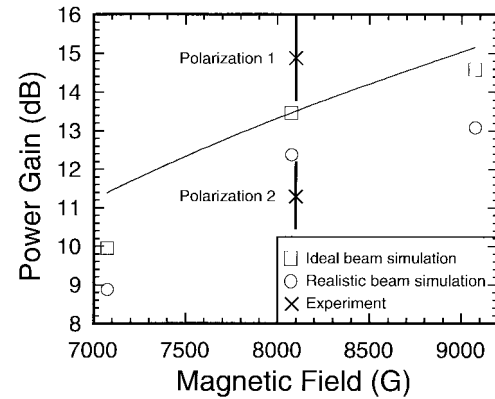


Fig. 4. Power gain (dB) versus axial magnetic field, B_0 (kG). Solid curve is from linear theory, squares and circles represent results of simulations with ideal beam and finite-emittance beam, respectively. Experimental results for the two polarizations are shown by crosses with vertical error bars.

the linearized theory. The squares represent the results of simulations with an ideal beam and the circles correspond to a finite-emittance initial distribution. The crosses indicate the least squares fits from the experimental data in Fig. 3 for the two linear polarizations, with the appropriate error bars. Linearized theory has higher gain than simulations, except for the synchronous case (the middle square in Fig. 4), where linearized theory and ideal beam simulations virtually agree. Over the range of magnetic field shown in Fig. 4 the gain is found to vary from ≈ 11 –15 dB. The experiments in [5] were

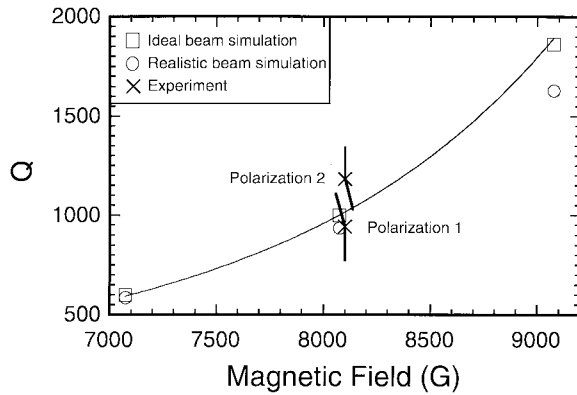


Fig. 5. Loaded Q versus axial magnetic field, B_0 (kG). Solid curve is from linear theory, squares and circles represent results of simulations with ideal beam and finite-emittance beam, respectively. Experimental results for the two polarizations are shown by crosses with error bars.

designed to operate as close as possible to the neutral point, i.e., the point with no beam loading. Given the error bars on the data the experimental points for the two polarizations are observed to bracket the theoretical results reasonably well.

Before proceeding it is necessary to remark on the cavity and drift-tube lengths in the simulations. For the synchronous case the lengths in the simulations are the same as those in the linear analysis and in Table I, with the drift tube being 1/2 of a cavity length. For nonzero detunings, however, it was found that the length of the drift tube was not optimal. For example, consider a highly detuned magnetic field $B_0 \approx 7$ kG. In this case there is a decrease in the gyrofrequency. As discussed prior to (5), the optimal length for the drift region is that which brings the electron from maximum excursion at the end of the drive cavity to the axis at the entrance to the gain cavity. This takes place in 1/2 of a gyroperiod. The reduced magnetic field thus necessitates a longer drift tube. As a result in the simulations the drift-tube length was optimized to be 3/4 of the cavity length—as opposed to 1/2 in the synchronous case. Similarly, for the example of $B_0 \approx 9$ kG, the drift-tube length was optimized to be 1/3 of the cavity length.

Fig. 5 shows the loaded Q as a function of the magnetic field. The solid curve is obtained from linear theory, the squares and the circles represent ideal beam and finite-emittance beam simulation results, respectively. This plot shows that a four-fold change in the quality factor may be effected by $\approx 25\%$ change in the magnetic field. Note that for magnetic field values below the synchronous value (see Table I) the loaded Q is less than the unloaded Q , and for magnetic field values above, the loaded Q is more than the unloaded Q . This is consistent with the theory in Sections II and III. Since the experiment operated near the point with no beam loading the experimental points in Fig. 5 show that the measured Q is close to the nominal Q listed in Table I and to the theoretical predictions.

Fig. 6 shows the predicted frequency shift as a function of the magnetic field. This plot shows that the resonant frequency is always down-shifted. That is, beam loading is capacitive, as pointed out in Section III. The experimental results are in reasonable agreement with theory.

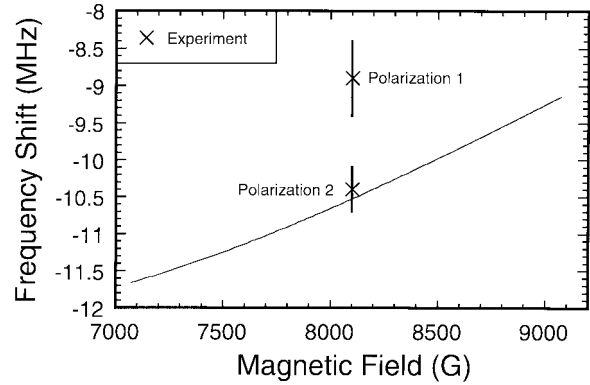


Fig. 6. Frequency shift (MHz) versus axial magnetic field, B_0 (kG). Solid curve is from linear theory. Experimental results for the two polarizations are shown by crosses with vertical error bars.

V. SUMMARY AND CONCLUSION

The role of beam loading in the deflection system of a magnetic-field-immersed magnicon has been analyzed. A first-principles analytical study, based on the Vlasov–Maxwell system of equations, leads to a very simple algebraic formula for the gain, from which the loaded Q (i.e., the instantaneous bandwidth) and the frequency shift may be obtained. This formula is derived by assuming that the interaction with the RF changes the electron energy by a small amount. Further, for simplicity, the gain formula is explicitly evaluated for an initially cold beam. It is shown that beam loading allows one to adjust the effective cavity Q very simply by varying the magnitude of the axial magnetic field. The cold-cavity Q can be halved or doubled by varying the magnetic field by $\sim 12.5\%$. Steady-state simulations of the deflection system are also presented to go beyond the regime of validity of the analytical theory, by allowing the electron energy to vary along the cavities and to incorporate the effects of finite beam emittance. When the magnetic field is chosen to be near the synchronous value the analytical results, simulations and the experiment agree fairly closely. However, at substantial detuning, the electron energy changes significantly and the agreement is no longer close. Away from synchronism the lengths of the cavities and drift tubes must be appropriately adjusted in order to optimize the gain.

In practice, experiments are invariably performed at magnetic fields below the synchronous value to avoid oscillation. Gain measurements at these magnetic fields will be the subject of a future paper.

REFERENCES

- [1] V. L. Granatstein and G. Nusinovich, "Criteria for comparing the suitability of microwave amplifiers for driving a TeV linear collider," in *IEEE Proc. Particle Acceleration Conf. 1991*, 1993, pp. 2572–2574.
- [2] V. L. Granatstein and C. D. Striffler, "Summary report: High intensity EM waves," in *AIP Conf. Proc. 279: Advanced Acceleration Concepts*, 1992, pp. 16–25.
- [3] M. M. Karliner, E. V. Kozyrev, I. G. Makarov, O. A. Nezhevenko, G. N. Ostreiko, B. Z. Persov, and G. V. Serdobintsev, "The magnicon—An advanced version of the gyrocon," *Nucl. Instrum. Methods Phys. Res.*, vol. A269, pp. 459–473, 1988.

- [4] W. M. Manheimer, "Theory and conceptual design of a high-power highly efficient magnicon at 10 and 20 GHz," *IEEE Trans. Plasma Sci.*, vol. 18, pp. 632–645, 1990.
- [5] S. H. Gold, C. A. Sullivan, B. Hafizi, and W. M. Manheimer, "Study of gain in C-band deflection cavities for a frequency-doubling magnicon amplifier," *IEEE Trans. Plasma Sci.*, vol. 21, pp. 383–387, 1993.
- [6] S. H. Gold, A. K. Kinkead, A. W. Fliflet, B. Hafizi, and W. M. Manheimer, "Initial operation of a high-power frequency-doubling X-band magnicon amplifier," *IEEE Trans. Plasma Sci.*, vol. 24, pp. 947–956, 1996.
- [7] B. Hafizi, Y. Seo, S. H. Gold, W. M. Manheimer, and P. Sprangle, "Analysis of the deflection system for a magnetic-field-immersed magnicon amplifier," *IEEE Trans. Plasma Sci.*, vol. 20, pp. 232–239, 1992.
- [8] B. Hafizi, S. H. Gold, W. M. Manheimer, and P. Sprangle, "Nonlinear analysis of a magnicon output cavity," *Phys. Fluids B*, vol. 5, pp. 3045–3055, 1993.
- [9] O. A. Nezhevenko, V. P. Yakovlev, S. H. Gold, and B. Hafizi, "Design of a high-power X-band magnicon amplifier," *IEEE Trans. Plasma Sci.*, vol. 22, pp. 785–795, 1994.
- [10] B. Hafizi and S. H. Gold, "Optimization studies of magnicon efficiency," *Phys. Plasmas*, vol. 2, pp. 902–914, 1995.
- [11] A. W. Fliflet and S. H. Gold, "Theory of competition between synchronous and nonsynchronous modes in a magnicon output cavity," *Phys. Plasmas*, vol. 2, pp. 1760–1765, 1995.
- [12] ———, "Mode competition in fourth-harmonic magnicon amplifiers," *IEEE Trans. Plasma Sci.*, vol. 24, pp. 957–963, 1996.
- [13] D. E. Rees, B. E. Carlsten, S. Humphries, and P. J. Tallerico, "Calculation of beam loading using the induced-current method in passive cavities," *IEEE Trans. Electron. Devices*, vol. 40, pp. 1543–1548, 1993.
- [14] R. E. Collin, *Foundations for Microwave Engineering*. New York: McGraw-Hill, 1992, ch. 7.
- [15] W. B. Herrmannsfeldt, "Electron trajectory program," Stanford Linear Accelerator Rep. no. 226, 1979.

B. Hafizi, photograph and biography not available at time of publication.



Steven H. Gold (M'86–SM'88–F'96) received the B.A. degree in physics from Haverford College, Haverford, PA, in 1968 and the M.S. and Ph.D. degrees in physics from the University of Maryland, College Park, in 1970 and 1978, respectively.

From 1978 to 1980 he held a National Research Council Resident Research Associateship with the Laser Plasma Branch of the Plasma Physics Division at the Naval Research Laboratory (NRL). During this time he studied energy transport through laser-accelerated thin-foil targets using optical diagnostic techniques. Since 1980 he has been a Research Physicist at NRL's Plasma Physics Division, where he has studied the generation of high-power coherent millimeter-wave and microwave radiation from gyrotrons, cyclotron autoresonance masers, and free-electron lasers driven by intense relativistic electron beams. He is presently working on the magnicon as a possible source of coherent radiation to power future linear colliders. He has published more than 40 papers and holds three patents and a Statutory Invention Registration. He served for five years as Supervisory Research Physicist and Head of the Intense Beam Microwave Generation Section of the Beam Physics Branch. His present position is Senior Scientist for Radiation Generation Physics. He is an Associate Editor of the *IEEE TRANSACTIONS ON PLASMA SCIENCE* and was Guest Editor of its Second Special Issue on High Power Microwave Generation in 1988.

Dr. Gold is a member of the IEEE Nuclear and Plasma Sciences Society and presently serves as Vice Chairman of the Executive Committee of its Plasma Science and Applications Committee. He is also a member of the Plasma Physics Division of the American Physics Society.